



# Global characteristics of ambient seismic noise

Xiaomeng Li · Yan Xu · Chaodi Xie · Shanshan Sun

Received: 22 April 2021 / Accepted: 23 December 2021 / Published online: 17 January 2022  
© The Author(s) 2022

**Abstract** Ambient seismic noise becomes more and more important and helpful on assisting velocity model inversion, earthquake detection, and ground motion prediction. Based on the analysis of continuous seismic data and ocean wave height, we find that the ocean wave height and winter storms have a controlling factor on the DF microseismic energy level and its frequency extent in time scale. It shows that high and low DF microseismic energy accompanied with wide and narrow frequency range consistent with the high wave height period (when the ocean is stormier) and low wave height period, respectively. Since DF microseism is dominated by Rayleigh waves, its energy attenuates very quickly when it travels through shoreline to the continent crust. Our observations give a quality factor  $Q$  of about 83 for DF energy traveling from the middle of the Atlantic to the central of Europe. We observe a lower energy

level of SPDF (short period DF) than that of LPDF (long period DF) for the continent stations, however a reversed situation for the island stations. It suggests that short period DF energy decays faster than the long period one. High-frequency ambient noise is called microtremor. The microtremor for the island station with low elevation has a semidiurnal modulation in phase with ocean tide. The microtremor for the station at other locations are from the anthropogenic activities which have diurnal, weekly, and annually variations.

**Keywords** Ambient seismic noise · Microseism · Microtremor · Frequency-dependent polarization analysis

## 1 Introduction

With the improvement of data storage and processing technique, the signal which has been regarded as noise for a long time has been used to inverse the crust and upper mantle velocity model (Shapiro et al. 2005; Yang et al. 2010), to predict the strong ground motion (Okada 2003; Denolle et al. 2014), and to improve the earthquake detection (Zhang et al. 2010). Ambient noise has become an important dataset for seismic studies.

Ambient seismic noise at period of 2 to 20 s generated by the standing waves in the ocean is named microseism (Gutenberg 1958). Hasselmann (1963)

---

X. Li · Y. Xu (✉) · C. Xie  
Department of Geophysics, Yunnan University, Kunming,  
Yunnan 650091, People's Republic of China  
e-mail: yanxu@ynu.edu.cn

X. Li  
Wenshan Zhuang and Miao Autonomous Prefecture  
Water Conservancy and Electric Power Survey  
and Design Institute, Wenshan, Yunnan, 663000,  
People's Republic of China

S. Sun  
Department of Atmospheric, Yunnan University,  
Kunming, Yunnan 650091, People's Republic of China

modeled the microseism at period of 12 to 20 s as a nonlinear coupling between the ocean wave and the shoal or the shallow water. The energy in this period is called the primary or single-frequency microseism (SF). The theory for the microseism at period of 6 to 10 s, called secondary or double-frequency microseism (DF), is the linear coupling between two trains of waves with the same frequency and moving toward each other (Longuet-Higgins, 1950). Noise at period around 0.5 to 2 s is documented as lake-generated microseism (Lynch 1952; Peterson 1993; Koper et al. 2009; Xu et al. 2017) which might have the similar generation theory as single and double frequency microseisms. The shorter period ambient seismic noise, approximately less than 1 s, is called microtremor mainly coming from the human activities (Gutenberg 1958; Asten 1978; Bonnefoy-Claudet et al. 2006). The frequencies of the microseism and microtremor cover the frequency band of body and surface waves.

No matter microseism or microtremor, their sources are not uniformly distributed, and their energy levels differ over the space and time. The non-uniformity of the source distribution and the difference of the energy level could bias the ambient noise

tomography, earthquake location, and strong ground motion prediction.

We analyze the continuous recordings on the globally distributed IRIS/IDA (II) stations using the polarization analysis technique and examine the frequency and polarization characters of the ambient seismic noise across the globe. For microseisms, we associate with the wind speed and ocean wave height from European Centre for Medium-Range Weather Forecasts (ECMWF) to provide the relationship between the seasonal and regional variation characters of microseismic noise and ocean motion. For microtremors, we investigate their characters with respect to the station locations.

## 2 Data and methodology

IRIS/IDA (II) network includes 45 broadband stations globally (Fig. 1). In order to extract the seasonal variation of the ambient seismic noise and to avoid the temporary changes, we download 3 years of continuous data, 2016 to 2018, from IRIS Data Management Center (DMC [www.iris.edu](http://www.iris.edu)). As station ARTI has been in operation since September 2018, station TLY

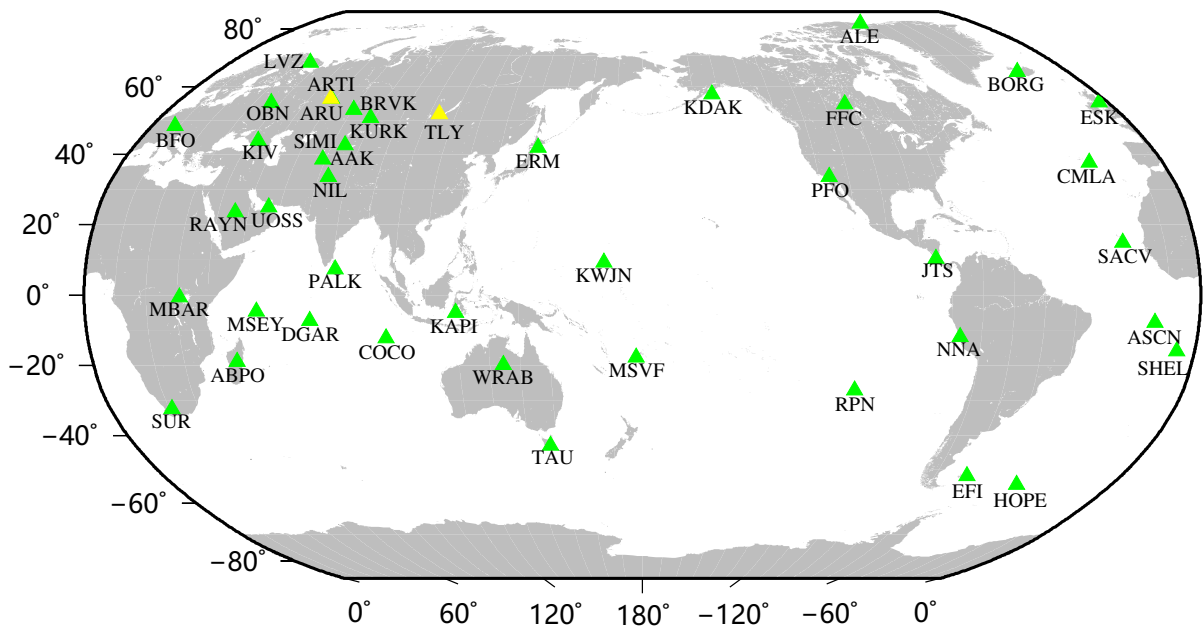


**Fig. 1** Locations of 45 II stations. Green triangles are the stations used. Yellow triangles are the stations not used. XPF has the same location as PFO. IBFO and XBFO have the same location as BFO

was closed due to the power problems in December 2015, and IBFO, XBFO, and XPFO have another instrument at the exact same location belonging to II,

these five stations are not used. Finally, three-component data (BHN, BHE, and BHZ) for 40 out of 45 stations are used in our study.

**Table 1** IRIS/IDA (II) network stations used in this study

Station	Latitude	Longitude	Elevation (m)	Used hours of data			Sampling rate	Instrument type
				2016	2017	2018		
AAK	42.64	74.49	1633	8685	8654	8679	40	STS-1 V/VBB
ABPO	-19.02	47.23	1528	8681	8627	8635	40	STS-1 V/VBB
ALE	82.50	-62.35	60	8302	8749	8743	40	STS-1 V/VBB
ARU	56.43	58.56	250	8742	8734	5924	20	STS-1 V/VBB
ASCN	-7.93	-14.36	173	8780	8646	8752	40	KS-54000
BFO	48.33	8.33	589	8762	8705	8733	20	STS-1 V/VBB
BORG	64.75	-21.33	110	8759	8747	8757	40	KS-54000
BRVK	53.06	70.28	330	8784	8540	8125	40	STS-1 V/VBB
CMLA	37.76	-25.52	429	8727	8733	8760	40	KS-54000
COCO	-12.19	96.83	1	8778	8586	8702	40	KS-54000
DGAR	-7.41	72.45	1	8604	8745	8760	40	STS-1 V/VBB
EFI	-51.68	-58.06	110	8721	8760	8666	40	KS-54000
ERM	42.01	143.16	40	8649	8760	8760	40	STS-1 V/VBB
ESK	55.32	-3.21	242	8784	8760	8760	40	STS-1 V/VBB
FFC	54.72	-101.98	338	5709	8753	8748	40	STS-1 V/VBB
HOPE	-54.28	-36.49	20	8510	7860	8743	40	Trillium240
JTS	10.29	-84.95	340	8747	7482	8261	40	STS-1 V/VBB
KAPI	-5.01	119.75	300	8681	8756	8645	40	KS-54000
KDAK	57.78	-152.58	152	7997	8690	8738	40	KS-54000
KIV	43.96	42.69	1054	8708	8746	8756	40	STS-1 V/VBB
KURK	50.72	78.62	184	8740	8520	8752	40	STS-1 V/VBB
KWJN	9.29	167.54	0	0	3664	8759	40	STS-5
LVZ	67.90	34.65	630	8783	8752	8754	40	STS-1 V/VBB
MBAR	-0.60	30.74	1390	8784	8290	8483	40	KS-54000
MSEY	-4.67	55.48	475	8722	8414	8310	40	KS-54000
MSVF	-17.74	178.05	801.1	8256	7602	7204	40	KS-54000
NIL	33.65	73.27	629	4667	7519	8338	40	KS-54000
NNA	-11.99	-76.84	575	8784	8746	8756	40	STS-1 V/VBB
OBN	55.11	36.57	160	8740	8682	8760	40	STS-1 V/VBB
PALK	7.27	80.70	460	8780	7611	7315	40	KS-54000
PFO	33.61	-116.46	1280	8756	8726	8729	40	STS-1 V/VBB
RAYN	23.52	45.50	631	8739	5268	8099	40	STS-2
RPN	-27.13	-109.33	110	8618	8067	8706	40	STS-1 V/VBB
SACV	14.97	-23.61	387	8782	8757	8759	40	KS-54000
SHEL	-15.96	-5.75	537	8784	8760	8760	40	KS-54000
SIMI	38.66	69.01	1400	1995	4620	8661	40	Trillium240
SUR	-32.38	20.81	1770	8784	8759	8758	40	STS-1 V/VBB
TAU	-42.91	147.32	132	8727	8759	8514	40	STS-1 V/VBB
UOSS	24.95	56.20	284.4	8783	8699	8066	40	STS-2.5
WRAB	-19.93	134.36	366	8773	8758	8507	40	KS-54000

Most of the stations are equipped with STS-1 V very broadband seismometer (Table 1). Some stations use KS-54000 ultra-low noise very broadband borehole seismometer. Few stations use Trillium 240, STS-2, or STS-5. Those broadband seismometers ensure our goal of analyzing the global characteristics of ambient noise at different frequency band. Continuous recording rate is above 80% for 37 out of 40 stations (Table 1). Since three stations, KWJN, SIMI, and NIL, with the lowest continuous recording rate can still guaranty at least a whole year of recordings, the missing data would not affect our results about seasonal variation.

We use frequency-dependent polarization analysis technique based on the eigen-decomposition of the 3-by-3 spectral covariance matrix (Koper and Hawley 2010; Park et al. 1987) to process the data. We remove the instrument response from the hour-long recordings downloaded from IRIS and restore them to ground accelerations. The hour-long data is used because transient events, e.g., small-to-moderate-sized regional earthquakes, will not affect the microseism observations (Sufri, et al., 2014). We try the different length of subwindow and find that 51.2 s window length can provide a smooth power spectral density curve and make a full use of the data. Each hour-long data is then divided into 69 subwindows with a length of 51.2 s and the adjacent subwindows overlap one another by 50%. Each subwindow is detrended and tapered with a Nuttall4c window defined with frequency limits of 0.005–0.01 Hz and 25–50 Hz. Fourier transform is applied on each component in each subwindow to obtain the corresponding spectrum  $y(f)$ . The 3-by-3 spectral matrix is given as

$$\frac{1}{K} M^H(f) \bullet M(f) \quad (1)$$

where

$$M(f) = \begin{bmatrix} y_0^{(1)}(f) & y_0^{(2)}(f) & y_0^{(3)}(f) \\ y_1^{(1)}(f) & y_1^{(2)}(f) & y_1^{(3)}(f) \\ \vdots & \vdots & \vdots \\ y_{K-1}^{(1)}(f) & y_{K-1}^{(2)}(f) & y_{K-1}^{(3)}(f) \end{bmatrix} \quad (2)$$

where the superscripts (1), (2), and (3) of  $y(f)$  represent the three components, the subscript 0 to  $K - 1$  indicates the number of the recordings, and  $H$  means the Hermitian conjugate transpose. Eigenvalue ( $\lambda$ )

and corresponding eigenvector can be obtained by proceeding the eigenvalue decomposition of the spectral matrix (1). The eigenvector corresponding to the largest eigenvalue includes the polarization feature, e.g., the horizontal azimuth. For each combination of time and station, the eigenvalue can be represented as the power spectral density (PSD), power spectrogram, and probability density function (PDF).

### 3 Results and discussion

#### 3.1 Seasonal characters of DF microseismic energy


We plot 3-year eigenvalues as spectrogram for all stations. Comparing ambient noise spectrograms (Fig. 2 and Fig. 3) with the ocean wave height data (Fig. 4), it is noticeable that the high wave height period in the northern or southern hemisphere has a clear controlling character on the DF microseismic energy (Stutzmann, et al., 2009; Hillers, et al. 2012).

The significant wave height in the northern hemisphere, between 30°N and 80°N, from ECWMF has an obviously seasonal change, low in local summer and high in local winter (Fig. 4). The southern hemisphere has broader ocean and less land area compared with the northern hemisphere. Due to this reason, the atmospheric movement in the southern ocean is a strong and stable circulation which causes the higher wave height and relatively less seasonal changes in this ocean region than in any other ocean area (Stutzmann, et al., 2009). Even the southern ocean has the highest wave height, its wave height also has the same seasonal change, low in local summer and high in local winter, as that in the northern hemisphere.

We can tell that DF microseisms have high energy levels during local winter and low energy levels during local summer for the stations in the northern hemisphere (Fig. 2). Since ocean wave heights are high in winter and low in summer in the north Pacific and Atlantic regions (Fig. 4), the DF microseismic energy level is highly correlated with the ocean wave height on time for the northern hemisphere.

The seasons in the southern hemisphere are opposite to those in the northern hemisphere. As a result of this conversion, the DF microseismic energy also has an opposite seasonal character compared to the results from the northern hemisphere, its high energy

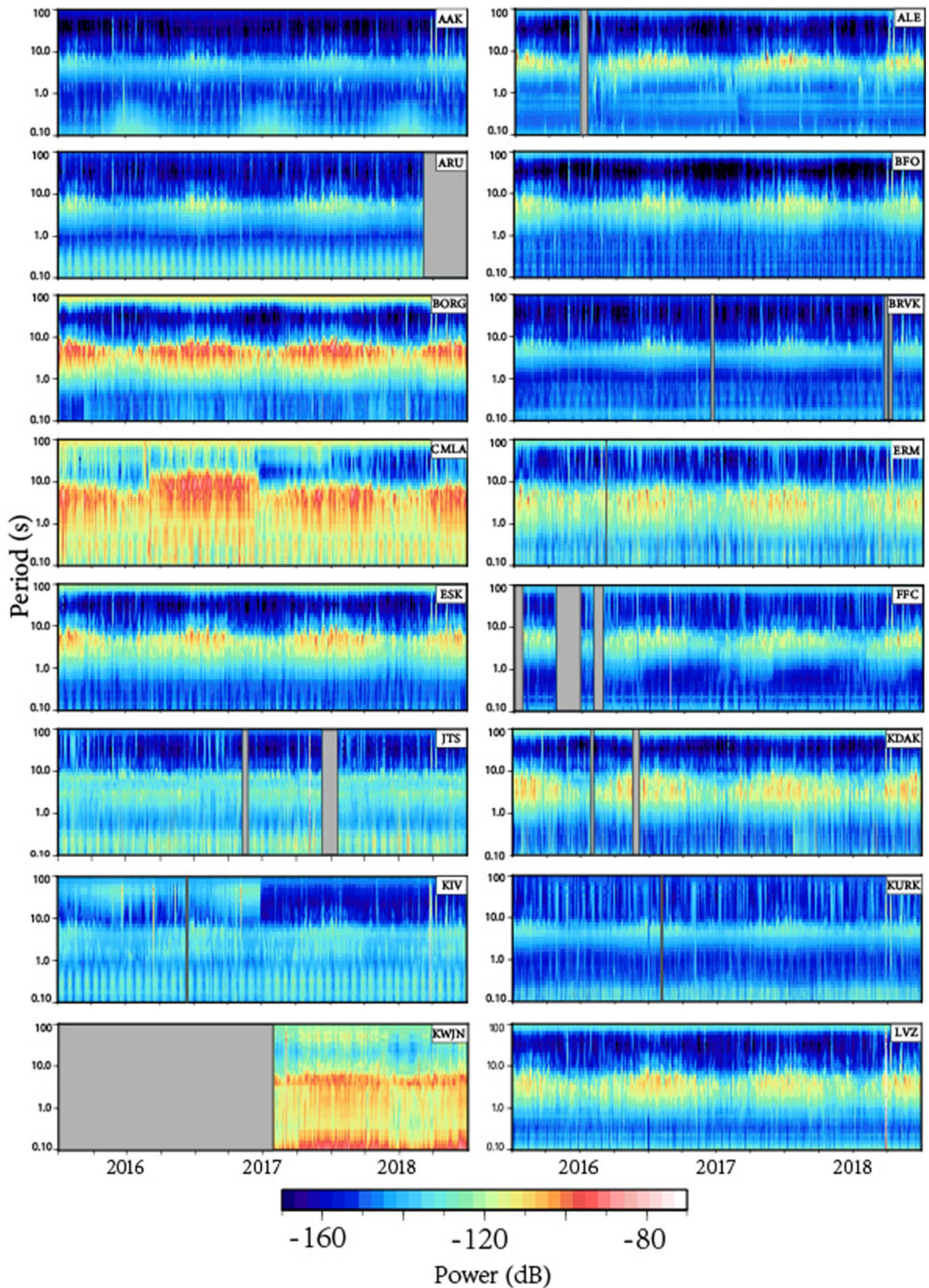


**Fig. 2** Spectrograms of the eigenvalues for the stations in the northern hemisphere. Gray blocks mark the time period without data. Station name is labeled on the upper right corner 

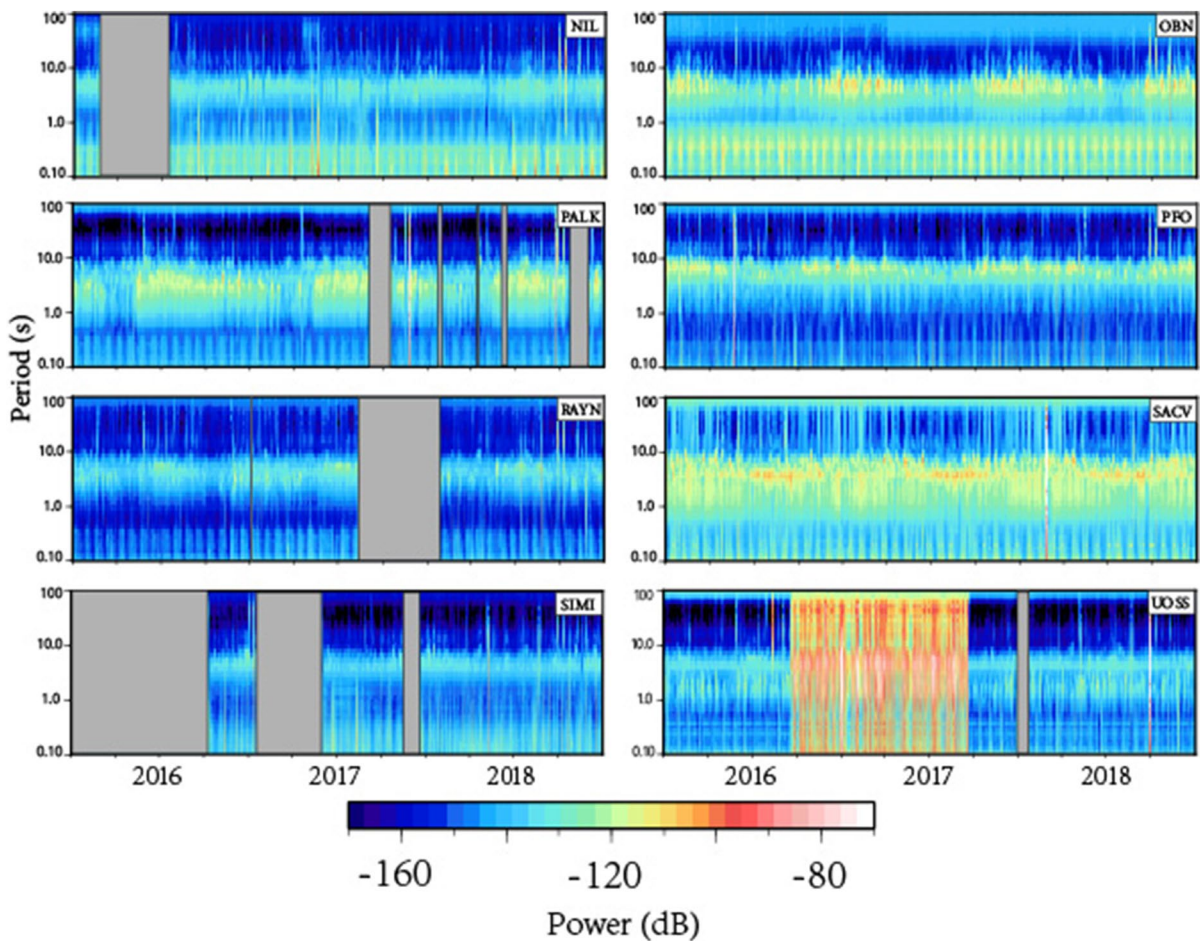


**Fig. 2** (continued)

time corresponds to the high wave height time in the southern ocean from 30°S to 80°S (Fig. 4).

Combining two hemispheres, we can find that no matter the northern or southern hemisphere, seismic DF microseisms show high and low energy during local winter and local summer, respectively, which is consistent with the results of Stutzmann et al. (2000), Aster et al. (2008), and Stutzmann et al. (2009).

There are three unique stations, UOSS, RAYN, and PALK. As they locate in the northern hemisphere, we expect the high DF energy during winter and low energy level during summer. However, these stations show a reversed DF energy level, low in winter and high in summer. In Fig. 2, we plot spectrograms for all 40 stations on the same color scale in order to compare the energy levels for the different geological units. Microseismic energies of these three

stations are clearly weaker than that of other stations. Besides that, since UOSS had instrument changing in between September 2016 and September 2017, its energy in this period is 30 dB higher than the energy in the remaining time (Fig. 2). As the character of the reverse DF energy level is not very clear using the same color scale, we replot three stations based on their own energy level in Fig. 5. Even UOSS, PALK, and RAYN locate in the northern hemisphere, DF energy shows high in summer and low in winter. UOSS and RAYN locate in the Arabian Peninsula and PALK locates in Sri Lanka, where are far away from the high wave height area in the northern hemisphere, the north Pacific and Atlantic regions, but close to the Arabian sea, northern Indian ocean. Significant wave height shows high wave during summer and low wave during winter in the Arabian sea (Fig. 4) with

the same dynamics as in southern hemisphere. This character is also observed by Koper et al. (2009). The time of high wave height in the Arabian sea correlates with the time of high DF energy, which suggests that the nearby open water has more influence on the DF microseismic energy for these three stations.

This result is reinforced by DF microseismic observations at stations near the southern ocean. Since the southern ocean has few lands, the atmospheric movement in the region is a strong and stable circulation which causes the higher wave height and relatively less seasonal changes in this ocean region than in any other ocean area. Due to this fact, some stations close to the southern ocean have high DF microseismic energy throughout the year without seasonal changes, e.g., station SUR, EFI, and HOPE in Fig. 3.

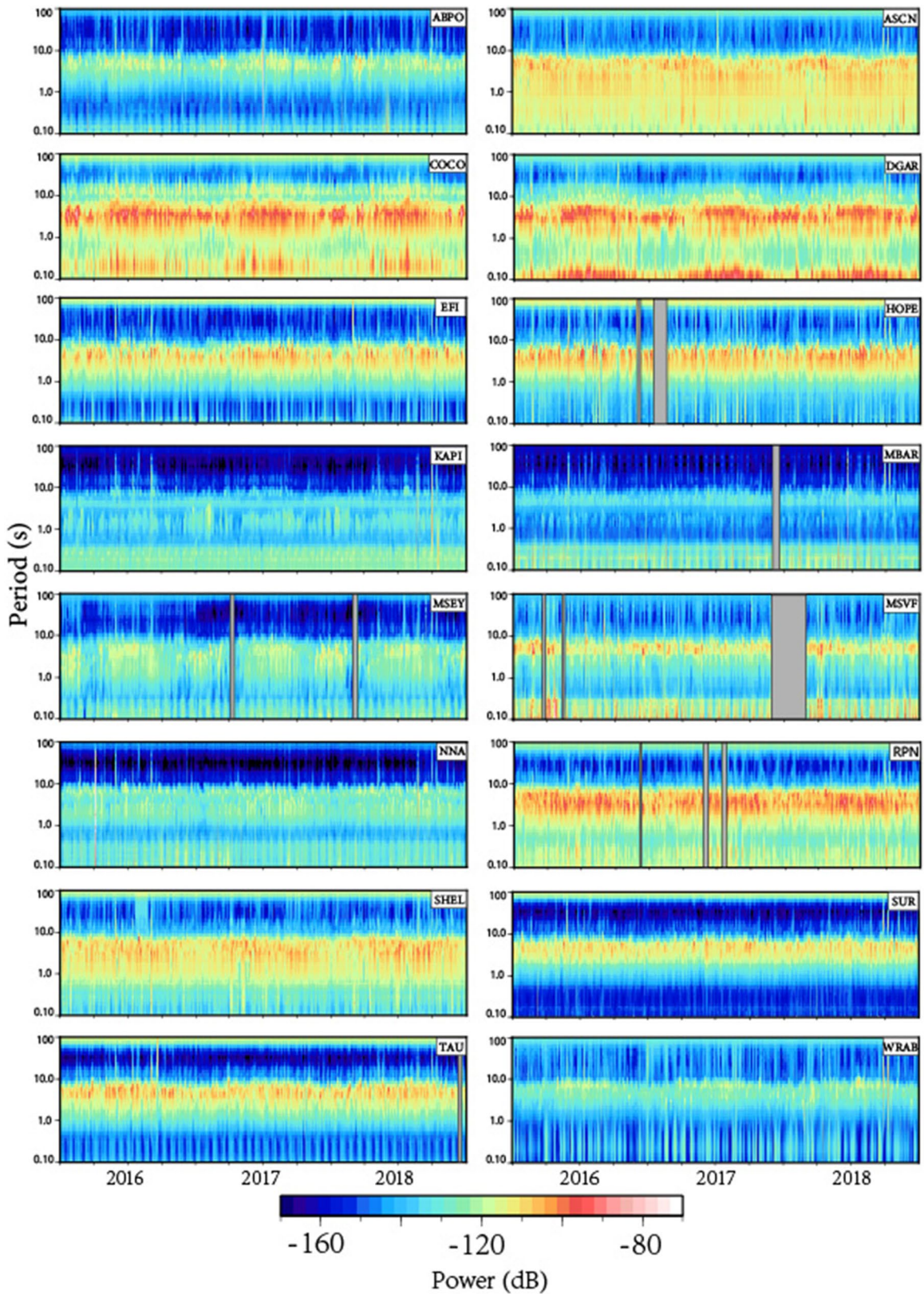
These observations refine the DF microseismic energy generation area. The DF microseismic energy comes from the nearby open water with high wave height. The north Pacific and north Atlantic control DF microseismic energies of most of stations in the northern hemisphere, showing high DF energy in winter and low energy level in summer. The Arabian sea controls DF microseismic energies of the nearby stations, which have high DF energy in summer and low in winter. The southern ocean controls DF microseismic energies of the stations in the southern hemisphere. There is no seasonal DF microseismic energy variation at stations very close to the southern ocean, but high DF energy all year long. Other stations in the southern hemisphere also have a seasonal DF microseismic energy variation, high in winter and low in summer. This correlation is consistent with the previous results, that is, the sources of the DF microseisms is related to the highest wave areas in the northern and southern hemisphere (Stutzmann et al., 2009). Besides the high wave height, the variations in microseismic power have been linked to the presence of ocean storms (Bromirski and Duennebieer 2002; Barrool et al. 2006; Gerstoft and Tanimoto 2007; Stutzmann et al. 2009). The climate perturbation transfers its energy to the water column through air-sea interactions to form the standing gravity waves that propagate to the ocean floor. This transferred energy increases significantly during large oceanic storms.

In addition to the consistence between the DF microseismic energy level and the seasonal wave height, the frequency range of the microseismic

energy has a fusiform shape which co-changes with the energy level and the ocean wave height, wide frequency range at its loop corresponding to the high DF energy and high wave height, and narrow frequency range at its node corresponding to the low DF energy and low wave height (Fig. 2). It might suggest that the high wave height can affect more coastal area and has more power to generate strong DF microseismic energy at a wider frequency range. This fusiform shape of the frequency range also relates to the storms. The energies shift toward longer periods during winter is due to the longer gravity wave produced by larger winter storms (Webb 1998; Stutzmann et al. 2000; Grob et al. 2011).

### 3.2 DF energy affected by the station location

BORG in Iceland, CMLA on Sao Miguel island, KWJN on Marshall islands, DGAR on Chagos islands, and COCO on Cocos islands are all island stations, which have the same DF character, high DF energy and broad frequency extent. As island broadly exposes to swell propagating from multiple source regions, which could end in broader DF microseismic energy frequency range and high energy (Aster 2008). DF energy is mainly radiated as Rayleigh wave which attenuates very quick when it travels through shoreline to the continent crust. The quality factor  $Q$  of surface waves can be expressed as  $Q = \frac{\pi f}{\alpha U}$ , where  $f$  is frequency,  $U$  is group velocity, and  $\alpha$  is the attenuation coefficient. We calculated the median daily DF peak energies of five stations from the island to the interior of Europe (Fig. 6). The median DF energies of five stations have the same fusiform shape, high in winter and low in summer, and gradually attenuate as the station location moving from the island to the inland. The median DF energy drops about 35 dB from the station BORG on island to the station AAK on inland, separated by about 7500 km, giving an attenuation coefficient  $\alpha$  of about 0.005 dB/km. Michell (1995) provided the attenuation coefficients  $\alpha$  of fundamental-mode Rayleigh waves at periods of 6~103 s for several study areas in the range of 0.0002~0.001 /km. Using an average Rayleigh wave group velocity of 1.25 km/s and frequency 6 s give a quality factor  $Q$  of about 83. This low





◀**Fig. 3** Spectrograms of the eigenvalue for the stations in the southern hemisphere. Gray blocks mark the time period without data. Station name is labeled on the upper right corner

$Q$  estimate is consistent with the study of amplitude variations of Rayleigh waves across a continental margin (McGarr, 1969) and reflects the high attenuation of DF energy along the long traveling path from the coast to the continent.

### 3.3 Polarization of the DF energy

Frequency-dependent polarization analysis technique will provide the information of spectral ground acceleration and its azimuthal orientation. The direction information can help analyze the relationship between the DF energy and the wave height. We plot the histogram of the azimuth of the peak DF energy for all stations and find that most stations have a dominant direction of DF peak energy, e.g., station ALE, ABPO, PFO, and SUR in Fig. 7. These directions do not necessarily point to the high wave height area, but to the nearby coast, which is consistent with the previous results that DF microseism is generated in the shallow water near the shoal rather than the deep ocean (Bromirski and Duennebier 2002; Bromirski et al. 1999).

Some inland stations, e.g., SIMI, KURK, and BRVK, have a wider azimuthal range. This character also happens to some island stations, ASCN, EFI, and SHEL. This wider azimuthal result informs that DF energies come from multiple sources in the surrounding oceans.

### 3.4 Splitted DF peak

Previous observations (Stephen et al. 2003; Bromirski et al. 2005, 2013) have found that DF microseism splits into two parts: LPDF (long-period DF about 0.085 to 0.2 Hz) and SPDF (short-period DF about 0.2 to 0.45 Hz). Not all stations can observe this splitting of the DF energy at any time. Five of our observations, JTS, KAPI, NNA, PALK, and SACV, can observe this DF energy splitting almost all year long (Figs. 2 and 8). The locations of five stations do not have a common factor, three out of five stations, KAPI, PALK, and SACV, on the island, another two stations, JTS and NNA, on the continent. Bromirski et al. (2005) suggested a strong correlation between

the high wind speed and the DF amplitude. However, none of five stations closes to any major high wind speed areas (Fig. 8). Bromirski et al. (2005) also found that nearshore local wave activity is the major source for SPDF and LPDF. Since SPDF and LPDF are both mainly propagating as Rayleigh waves, and the short period energy attenuates faster than the long period one when the signals travel to the land, we can see that the SPDF energy is higher than the LPDF energy for three island stations (Fig. 8a, b, and c) and is lower than the LPDF energy for two land stations, JTS and NNA (Fig. 8e, f).

### 3.5 Microtremor characters

Noise with periods less than 1 s is named microtremor. Since seismic station noise levels vary with geographic location (Peterson 1993; Reif et al. 2002; Stutzmann et al. 2000; McNamara and Buland 2004), microtremor has a clearly regional character.

Ocean is one of the primary contributors to microtremor (Webb 1998; McNamara and Buland 2004). COCO, DGAR, and KWJN are all on the island with 0 km or 1 km station elevation (Table 1). The microtremors of three stations are at least 20 dB higher than those of other stations (Figs. 2 and 3) and appear the same characters as the DF microseism, high energy level during summer and low energy level during winter, and a half fusiform shape of frequency range co-changing with energy level. These characters suggest that microtremors at these stations are controlled by the high wave height in the north Pacific and southern ocean like the DF microseism. Especially, microtremor energy at KWJN station has a semidiurnal modulation in phase with ocean tide (Fig. 9). As we cannot find the tide observation at the KWJN station, we plot microtremor energy in between May 14 to May 20 2018 from KWJN station against the observed ocean tide from the nearby Apia port, Samoa. Since the tide observation is available since July 2019, we download the tide data with the same time period in 2020 instead of in 2018, from National Marine Data and Information Service, NMDIS, <http://global-tide.nmdis.org.cn/Default.html>. Microtremor from KWJN station has two peaks approximately separated with 12 h. Ocean tide also has two high tides every day and highly correlates with microtremor high energy in time. The similar semidiurnal

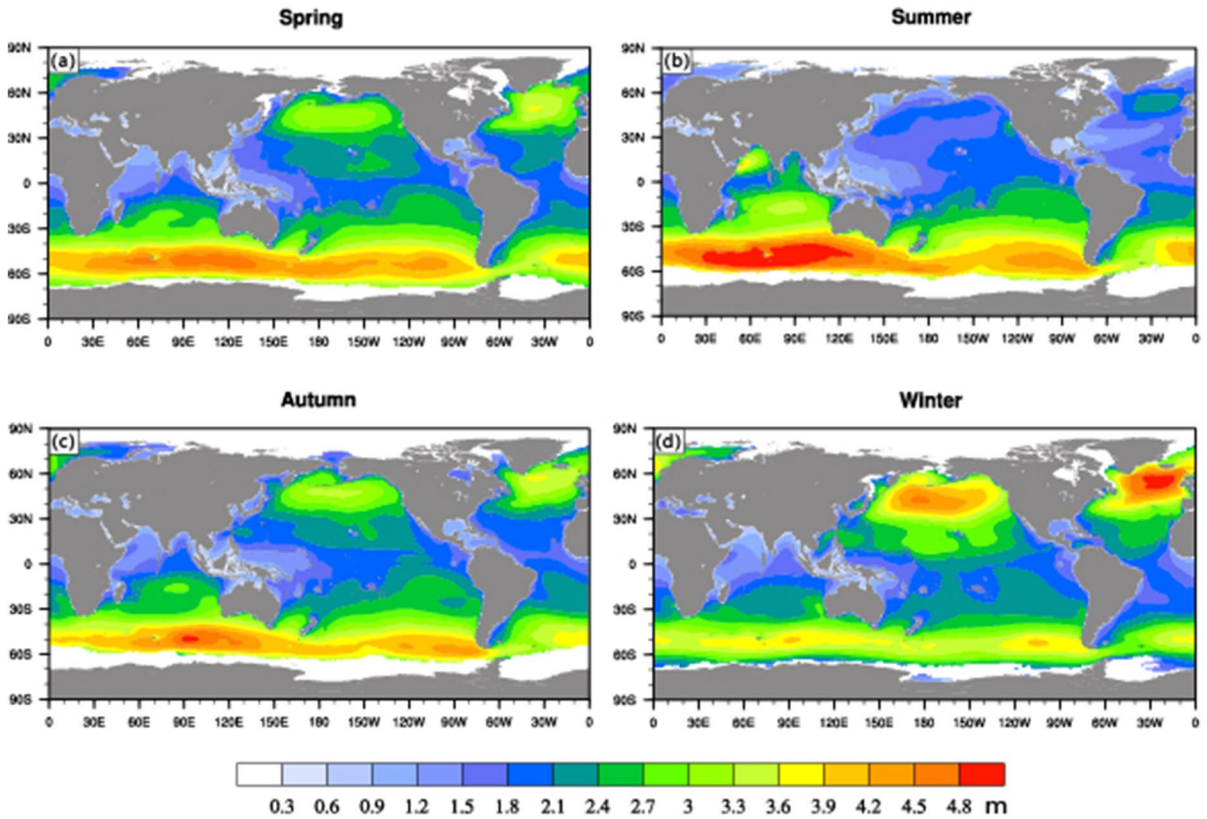


**Fig. 4** Seasonal averaged significant wave height over 3 years for **a** spring (Mar–Apr–May), **b** summer (Jun–Jul–Aug), **c** autumn (Sep–Oct–Nov), and **d** winter (Dec–Jan–Feb) from European Centre for Medium-Range Weather Forecasts (ECMWF)

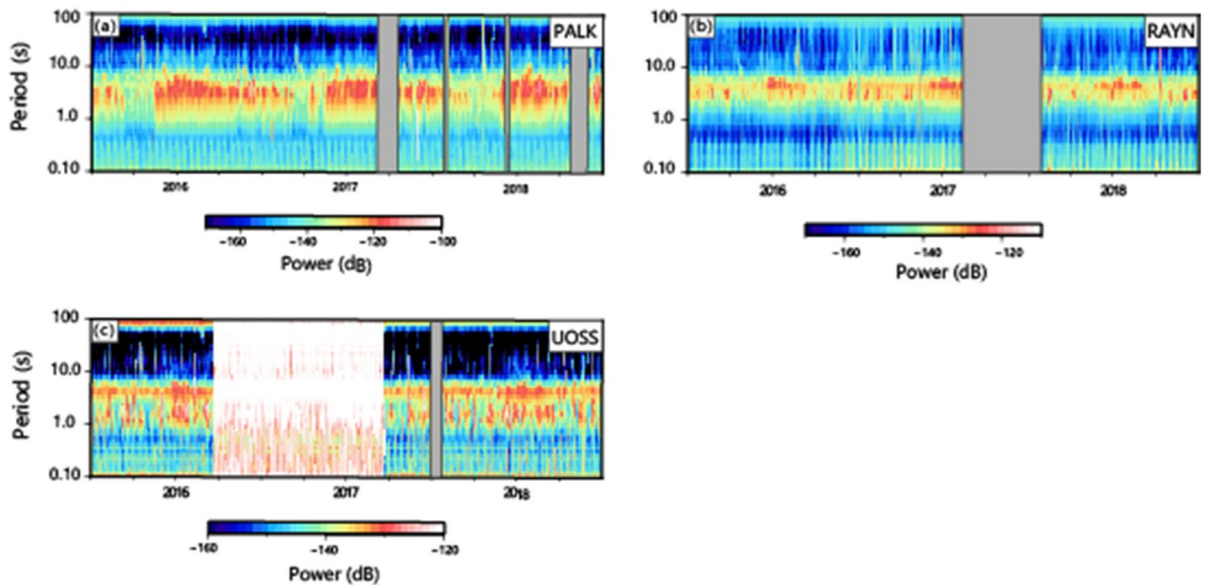


**Fig. 5** Spectrograms for stations around the Arabian sea. Gray blocks mark the time without data

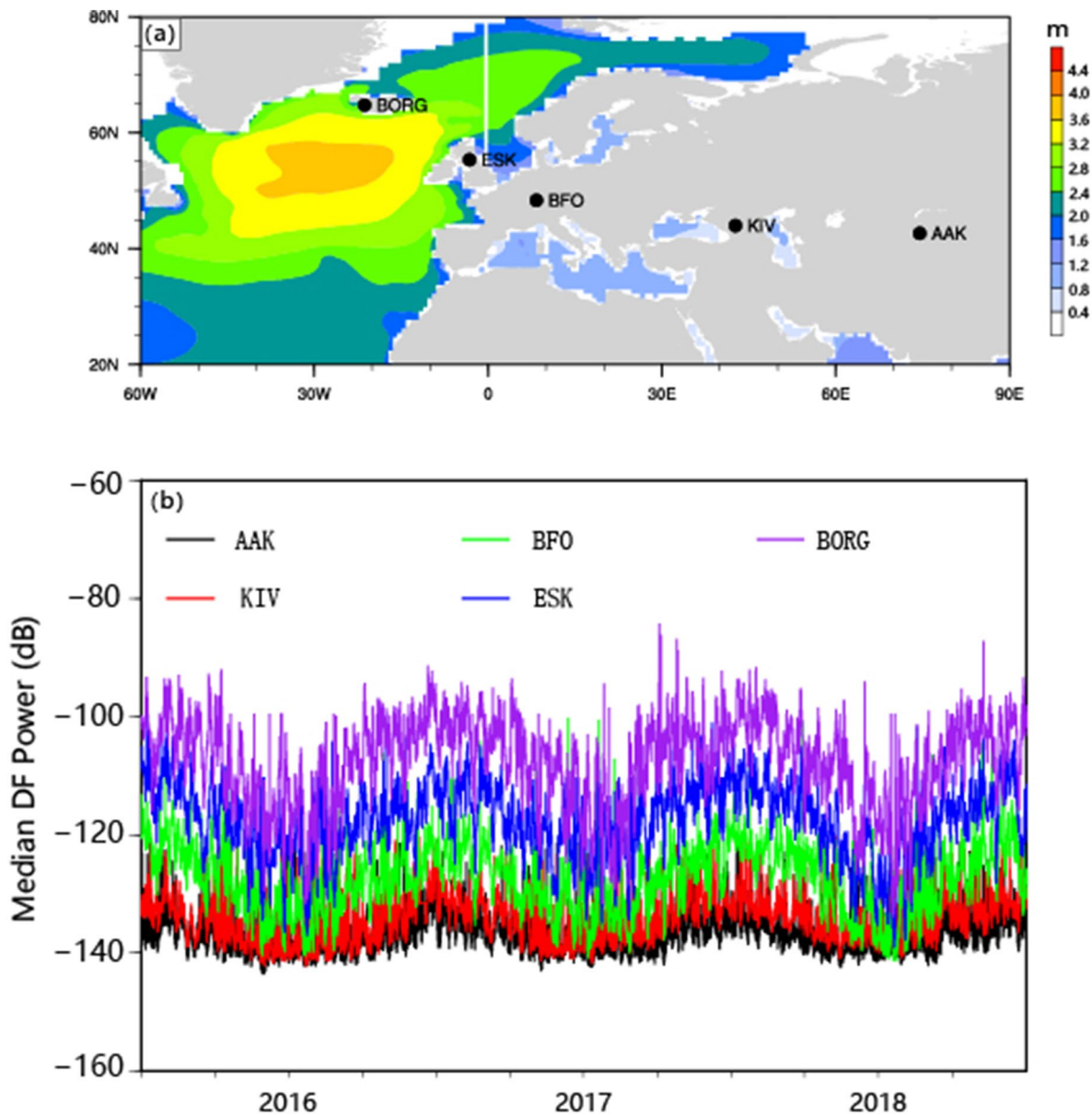


**Fig. 6** **a** Three years mean significant wave height in the Atlantic and the locations of five seismic stations in Europe. **b** Median daily DF peak energies at five seismic stations

modulation in phase with tides is observed for the infragravity wave energy, which is interpreted as the result of nonlinear transfers of energy from low-frequency long waves to higher-frequency motions, microseisms (Thomson et al. 2006; Dolenc et al. 2008). When the waves propagate over the convex low-tide beach profile than over the concave high-tide profile, the observed infragravity waves have

less energy at low tides (Thomson et al. 2006). Our microtremor energy having a semidiurnal modulation in phase with ocean tide shows that the similar mechanism for the infragravity waves could reach to higher frequency band. Microtremors generated by the ocean waves attenuated very quickly with increasing the elevation as this high-frequency energy propagates mainly as high-frequency surface

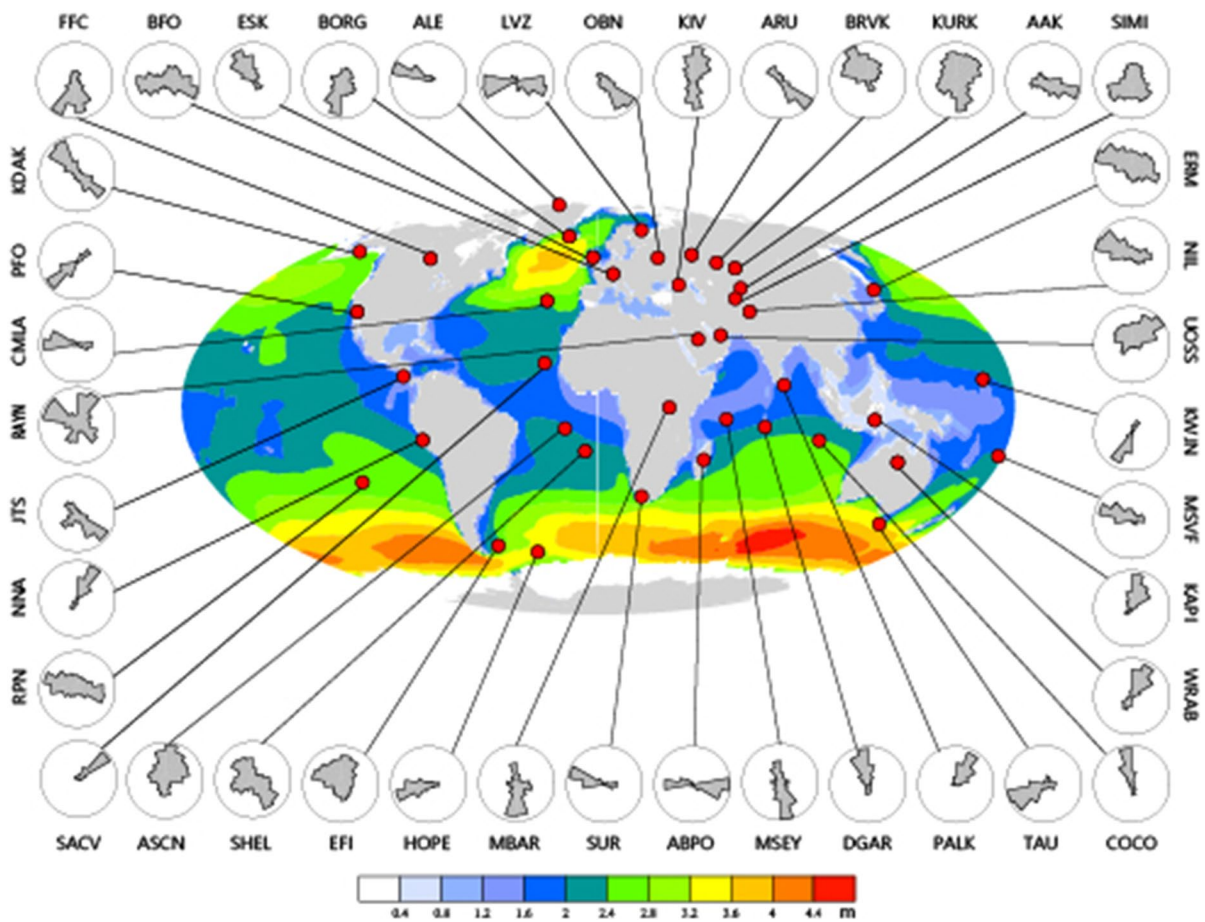


**Fig. 7** Three years mean significant wave height and the distribution of back azimuths estimated for DF microseisms at 40 stations. Red dots are the location of stations

waves that attenuate within several kilometers in distance and depth (McNamara and Buland 2004). HOPE and RPN are both on island with station elevations of 40 and 110 m, respectively. Their microtremor energies are clearly lower than that of the island stations, COCO, DGAR, and KWJN (Fig. 2).

In addition to the noise generated by the ocean, anthropogenic activities are another important source for the microtremor. Microtremors caused by the anthropogenic activities have obvious diurnal, weekly, and seasonal variations (McNamara and Buland 2004; Bonnefoy-Claudet et al. 2006; Anthony et al. 2015). For example, AAK station locates near the Ala Archa National Park in Kyrgyzstan. This national park opens all year round, with the best visiting time from the end of spring to the beginning of the autumn. Our microtremors show a very obvious

seasonal change, high in summer and autumn and low in spring and winter, which is consistent with the anthropogenic seasonal characters of visiting the national park (Fig. 2). ALE station is in Alert, N. W. T, Canada, where is inside the Arctic circle with Polar day from last week of March till mid-September and Polar night from mid-December till end of February. Microtremor of ALE station is quiet during January 2018 and noisy during August 2018 (Fig. 10a,b), consistent with the Polar day and Polar night time. The clear high energies in January 2018 are associated with the earthquakes occurred globally (Fig. 10a). BFO station is in the Black Forest, Schiltach, Germany. On the 3-year scale shown in Fig. 2, it is difficult to find the diurnal and weekly characters of microtremor. Zooming into 0.11 to 0.25 s and only plotting 2 weeks' data, we can see a clear behavior

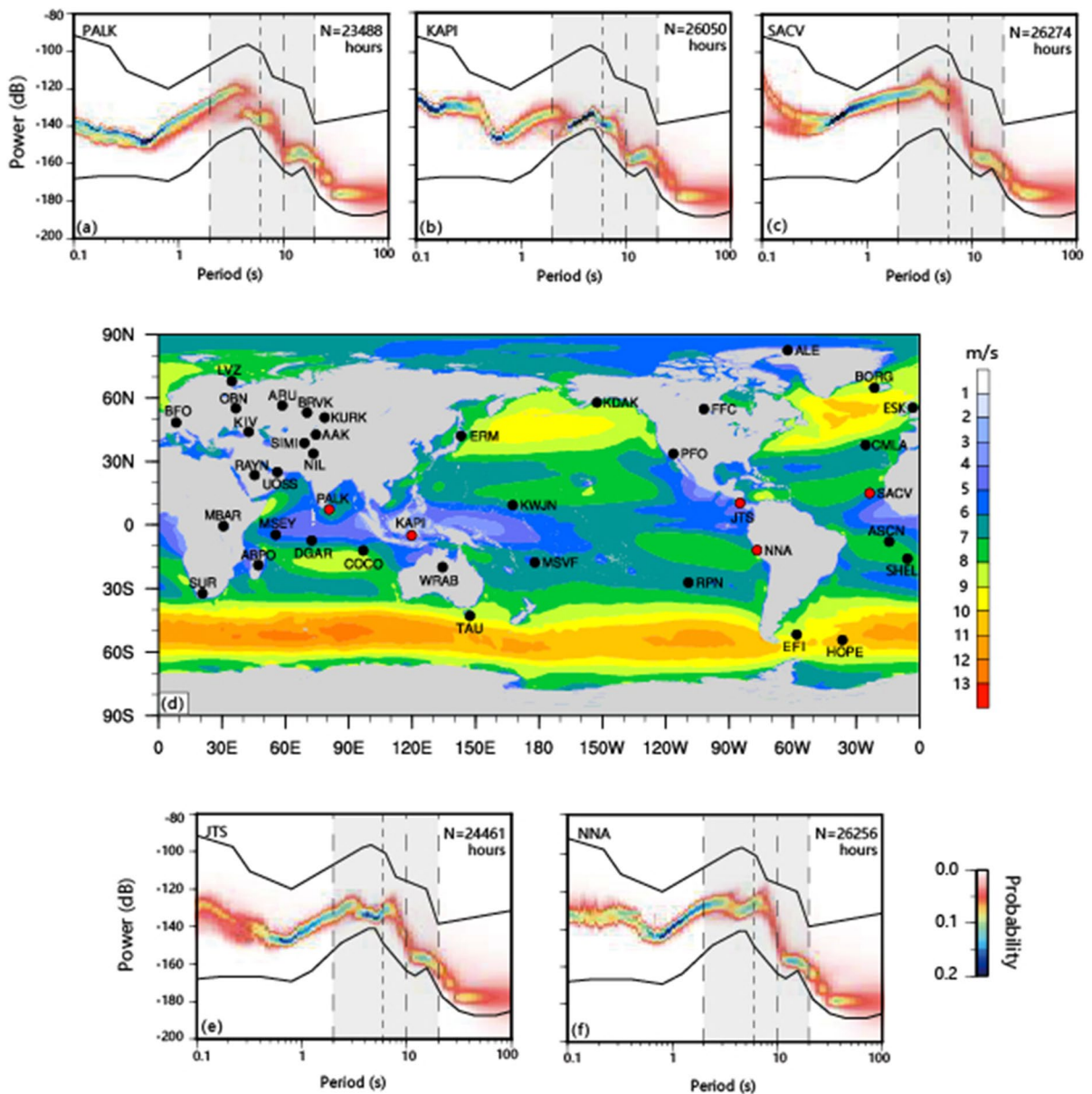


**Fig. 8** Probability density functions (PDF) for ambient seismic noises of the eigenvalue for five stations, **a** is for station PALK, **b** is for station JTS, **c** is for SACV, **e** is for KAPI, and **f** is for NNA, from 2016 to 2018. The black lines are the low and high reference models of Peterson (1993). Power is measured in decibel units (dB) of spectral acceleration. **d** is 3 years median wind speed and the location of 40 seismic stations,

black and red circles. Red circles represent the location of five stations showing PDF in **(a)**, **(b)**, **(c)**, **(e)**, and **(f)**. The grey-shaded area indicates the microseism band of 2–20 s, and the dashed vertical lines divide this into single-frequency (SF, 10–20 s) and double-frequency (DF, 2–10 s) bands. The dotted vertical line divides the DF band into short-period (SPDF, 2–6 s) and long-period (LPDF, 6–10 s) bands

of the weekly anthropogenic activities near the BFO station, Fig. 10c. Monday to Friday are the work days, correspondingly high energy levels are observed in the high-frequency band. Microtremor on Saturday

morning shows some relatively weaker human movements compared to the energy level on weekdays and stops around 12 am. Microtremor reveals a quiet anthropogenic activity continuing from Saturday

**Fig. 9** Comparison of the microtremor spectrogram at station KWJN in between May 14 and May 20 2018 with the observed tide at the nearby Apia port in Samoa, black line, in the same time period in 2020

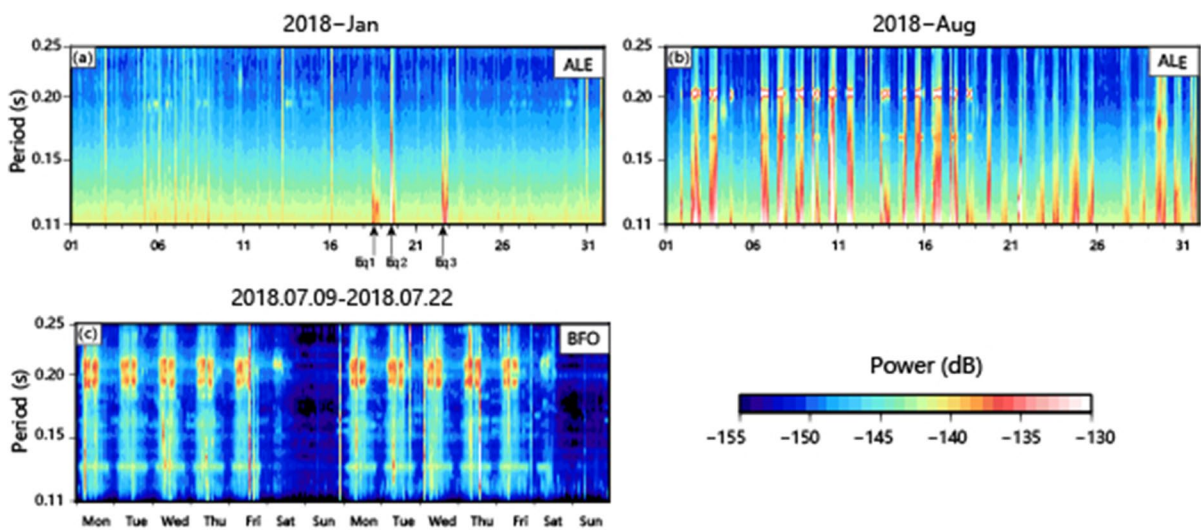
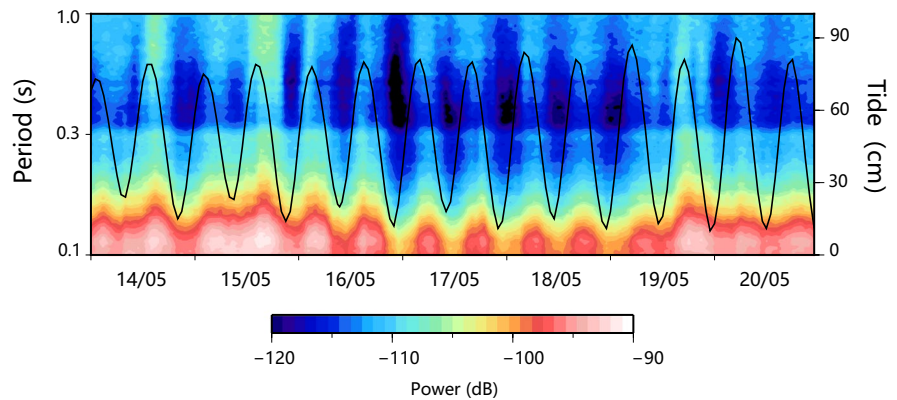


**Fig. 10** The microtremor spectrogram during Polar night (January in 2018) (a) and Polar day (August in 2018) (b) at ALE station. The earthquakes larger than Mw 5.0 or Mb 5.0 occurred globally during January 2018 are marked on (a) with labels Eq. 1, Eq. 2, and Eq. 3. Equation 1: 2018–01–18

12:08:52, Northwest of Kuril Islands, Mw 5.7 and 2018–01–18 17:48:39, Indonesia, Mw 5.6; Eq. 2: 2018–01–19 16:17:42, Gulf of California, Mw 6.3; Eq. 3: 2018–01–22 19:39:58, Central Mid-Atlantic Ridge, Mb 5. c Diurnal and weekly characters of microtremor at BFO station from July 9<sup>th</sup> to 22<sup>nd</sup>, 2018

afternoon to Sunday. Except this weekly behavior of anthropogenic activities, BFO also records the diurnal anthropogenic behavior. Microtremor at about 0.2 s rises sharply at 5 am, appears an obvious gap at noon, and drops sharply at 5 pm. The time line of the noise level highly correlates with the working pattern.

#### 4 Conclusions

By analyzing three years of data from 40 three-component long operating stations and ocean wave height,

we find that DF microseismic energy level and its frequency extent mainly controlled by the ocean wave height and winter storms. Most of the stations in the northern and southern hemispheres have high energy level and wide frequency extent in winter and low energy level and narrow frequency extent in summer consistent with the high ocean wave height time in the north Pacific, north Atlantic, and the southern ocean, respectively. The time of high wave height in the Arabian sea is different from that in other oceans, which causes the DF microseismic energy of stations around the Arabian sea to be more affected by this sea area

than by the north Pacific and north Atlantic. The station near the Arabian sea has DF low energy level and narrow frequency extent in winter which is opposite from other stations in the northern hemisphere. Due to the high wave height through the whole year in the southern ocean, the station closes to this ocean area does not have a clear seasonal variation of DF microseismic energy and frequency extent. Even the north Pacific, north Atlantic, and southern ocean control the DF energy in time scale, the direction of the peak DF microseismic energy does not point to the high wave height area but points to the nearby coast region. The polarization information suggests that the DF microseismic energy comes from the nearby coast area. As DF microseism is mainly radiated as Rayleigh wave, its energy attenuates very quick when it travels through shoreline to the continent crust. The stations from the middle of the Atlantic to the central of Eurasia plate give a quality factor  $Q$  of about 83. Owing to the same reason, short period DF energy decays faster than the long period one. We observe a lower energy level of SPDF (short period DF) than that of LPDF (long period DF) for the continent stations however a reversed situation for the island stations.

Microtremor is mainly generated by the ocean for the island station with elevation close to or equal to the sea level and attenuates pretty quick with increasing the station elevation. Anthropogenic activity is another major source of microtremor, which has diurnal, weekly, and annual variations.

**Acknowledgements** The authors would like to thank the anonymous reviewer and the editorial staff for their helpful comments. This work was supported by the National Science Foundation of China under awards 41564003, 41964001 and 42005122.

#### Declarations

**Conflict of interest** The authors declare no competing interests.

**Open Access** This article is licensed under a Creative Commons Attribution 4.0 International License, which permits use, sharing, adaptation, distribution and reproduction in any medium or format, as long as you give appropriate credit to the original author(s) and the source, provide a link to the Creative Commons licence, and indicate if changes were made. The images or other third party material in this article are included in the article's Creative Commons licence, unless indicated otherwise in a credit line to the material. If material is not included in the article's Creative Commons licence and your intended use is not permitted by statutory regulation or exceeds

the permitted use, you will need to obtain permission directly from the copyright holder. To view a copy of this licence, visit <http://creativecommons.org/licenses/by/4.0/>.

#### References

- Anthony RE, Aster RC, Wiens D, Nyblade A, Anandkrishnan S, Huerta A et al (2015) The seismic noise environment of antarctica. *Seismol. Res. Lett.* 86(1):89–100. <https://doi.org/10.1785/0220140109>
- Asten MW (1978) Geological control of the three-component spectra of Rayleigh-wave microseisms. *Bull Seismol Soc Am* 68(6):1623–1636
- Aster CR, McNamara DE, Bromirski PD (2008) Multidecadal climate-induced variability in microseisms. *Seismol Res Lett.* <https://doi.org/10.1785/gssrl.79.2.194>
- Barruol G, Reymond D, Fontaine FR, Hyvernaud O, Maurer V, Maamaatuaiahutapu K (2006) Characterizing swells in the southern Pacific from seismic and infrasonic noise analyses. *Geophys J Int* 164:516–542. <https://doi.org/10.1111/j.1365-246X.2006.02871.x>
- Bonnefoy-Claudet S, Cotton F, Bard P (2006) The nature of noise wavefield and its applications for site effects studies, A literature review. *Earth Sci Rev* 79:205–227. <https://doi.org/10.1016/j.earscirev.2006.07.004>
- Bromirski PD, Duennebieer FK (2002) The near-coastal microseism spectrum: spatial and temporal wave climate relationships. *J. Geophys. Res.* 107(B8):265. <https://doi.org/10.1029/2001JB000265>
- Bromirski PD, Flick R, Graham N (1999) Ocean wave height determined from inland seismometer data: implications for investigating wave climate changes in the NE Pacific. *J Geophys Res* 104:20753–20766
- Bromirski PD, Duennebieer FK, Stephen RA (2005) Mid-ocean microseisms. *Geochem Geophys Geosyst* 6:Q04009. <https://doi.org/10.1029/2004GC000768>
- Bromirski PD, Stephen RA, Gerstoft P (2013) Are deep-ocean-generated surface-wave microseisms observed on land? *J Geophys Res Solid Earth* 118:3610–3629. <https://doi.org/10.1002/jgrb.50268>
- Denolle MA, Dunham EM, Prieto GA, Beroza GC (2014) Strong ground motion prediction using virtual earthquakes. *Science* 343:399–403
- Dolenc D, Romanowicz B, McGill P, Wilcock W (2008) Observations of infragravity waves at the ocean-bottom broadband seismic stations Endeavour (KEBB) and Explorer (KXBB). *Geochem Geophys Geosyst* 9:Q05007. <https://doi.org/10.1029/2008GC001942>
- Gerstoft P, Tanimoto T (2007) A year of microseisms in southern California. *Geophys Res Lett* 34:L20304. <https://doi.org/10.1029/RG001i002p00177>
- Grob M, Maggi A, Stutzmann E (2011) Observations of the seasonality of the Antarctic microseismic signal, and its association to sea ice variability. *Geophys Res Lett* 38:L11302. <https://doi.org/10.1029/2011GL047525>
- Gutenberg B (1958) Microseisms. *Adv Geophys* 5:53–92
- Hillers G, Graham N, Campillo M, Kedar S, Landès A, Shapiro N (2012) Global oceanic microseism sources as seen

- by seismic arrays and predicted by wave action models. *Geochem Geophys Geosyst* 13:Q01021. <https://doi.org/10.1029/2011GC003875>
- Koper KD, Hawley VL (2010) Frequency dependent polarization analysis of ambient seismic noise recorded at a broadband seismometer in the Central United States. *Earthquake Sci* 23(439–447):B10310. <https://doi.org/10.1029/2009JB006307>
- Koper KD, de Foy B, Benz H (2009) Composition and variation of noise recorded at the Yellowstone Seismic Array, 1991–2007. *J Geophys Res* 114(B10):307
- Longuet-Higgins M (1950) Theory on the origin of microseisms. *Philos Trans R Soc London Ser A* 243:1–35
- Lynch J (1952) The Great Lakes, a source of two-second frontal microseisms. *EOS Trans Am Geophys Union* 33(3):432–434. <https://doi.org/10.1029/TR033i003p00432>
- McGarr A (1969) Amplitude variations of Rayleigh waves-propagation across a continental margin. *Bull Seismol Soc Am* 59(3):1281–1305
- Mcnamara DE, Buland RP (2004) Ambient noise levels in the Continental United States. *Bull Seismol Soc Am* 94(4):1517–1527
- Mitchell BJ (1995) Anelastic structure and evolution of the continental crust and upper mantle from seismic surface wave attenuation. *Rev Geophys* 33(4):441–462
- Okada, H., 2003. The microtremor survey method, Geographical Monograph Series Vol. 12, Society of Exploration Geophysicists with the cooperation of Society of Exploration Geophysicists of Japan and Australian Society of Exploration Geophysicists.
- Park J, Vernon FL, Lindberg CR (1987) Frequency dependent polarization analysis of high-frequency seismograms. *J Geophys Res Solid Earth* 92(B12):12664–12674
- Peterson, J., 1993. Observation and modeling of seismic background noise (95 pp.). *U.S. Geol. Surv. Open-File Rept.* 93–322
- Reif C, Shearer PM, Astiz L (2002) Evaluating the performance of global seismic stations. *Seismol Res Lett* 73(1):46–56
- Shapiro NM, Campillo M, Stehly L, Ritzwoller MH (2005) High-resolution surface-wave tomography from ambient seismic noise. *Science* 307(5715):1615–1618. <https://doi.org/10.1126/science.1108339>
- Stephen RA, Speiss FN, Collins JA, Hildebrand JA, Orcutt JA, Peal KR, Vernon FL, Wooding FB (2003) Ocean seismic network pilot experiment. *Geochem Geophys Geosyst* 4(10):1092. <https://doi.org/10.1029/2002GC000485>
- Stutzmann E, Roult G, Astiz L (2000) Geoscope station noise level. *Bull Seismol Soc Am* 90:690–701. <https://doi.org/10.1785/0119990025>
- Stutzmann E, Schimmel M, Patau G, Maggi A (2009) Global climate imprint on seismic noise. *Geochem Geophys Geosyst* 10:Q11004. <https://doi.org/10.1029/2009GC002619>
- Sufri O, Koper KD, Burlacu R, de Foy B (2014) Microseisms from Superstorm Sandy. *Earth Planet Sci Lett* 402:324–336
- Thomson J, Elgar S, Raubenheimer B, Herbers THC, Guza RT (2006) Tidal modulation of infragravity waves via nonlinear energy losses in the surfzone. *Geophys Res Lett* 33:L05601. <https://doi.org/10.1029/2005GL025514>
- Webb SC (1998) Broadband seismology and noise under the ocean. *Rev Geophys* 36:105–142
- Xu Y, Koper KD, Burlacu R (2017) Lakes as a source of short-period (0.5–2 s) microseisms. *J. Geophys. Res. Solid Earth* 122:8241. <https://doi.org/10.1002/2017JB014808>
- Yang Y, Zheng Y, Chen J, Zhou S, Ceylan S et al (2010) Rayleigh wave phase velocity maps of Tibet and the surrounding regions from ambient seismic noise tomography: Rayleigh wave phase velocities in Tibet. *Geochem. Geophys. Geosyst.* 11(8):119. <https://doi.org/10.1029/2010GC003119>
- Zhang J, Gerstoft P, Shearer PM (2010) Resolving P-wave travel-time anomalies using seismic array observations of oceanic storms. *Earth and Planet Sci Lett.* <https://doi.org/10.1016/j.epsl.2010.02.014>

**Publisher's note** Springer Nature remains neutral with regard to jurisdictional claims in published maps and institutional affiliations.